Selective Adsorptive Separation of Carbon Dioxide and Methane on a Tetraethylenepentamine-Impregnated Solid Sorbent

Yu Zhou[1*], Xiaoping Jiang[1], Zhe Tang[2], Mingyang He[1] and Qi Xu[2]

[1]College of Chemistry and Chemical Engineering, Changzhou University, Changzhou, Jiangsu Province, China
[2]School of Chemical and Biological Engineering, Yancheng Institute of Technology, Yancheng, Jiangsu Province, China

_____

ABSTRACT

To achieve selective CO_2 adsorption, the ordered mesoporous material Na-MCM-41 was synthesized by a hydrothermal method and subsequently modified with different amounts of tetra ethylene pentamine (TEPA) through wet impregnation. The as-synthesized adsorbents were characterized by Fourier transform infrared spectroscopy, X-ray diffraction, BET analysis, energy-dispersive X-ray spectroscopy, and transmission electron microscopy. The effects of amine loading and adsorption temperature on the performance of the adsorbents for selective CO_2 adsorption were evaluated using a breakthrough method with a fixed-bed reactor equipped with an online multicomponent gas analyzer. The CO_2 adsorption capacity of Na-MCM-41 with 55 wt.% TEPA loading (Na-MCM-41(0.55)) was as high as 3.178 mmol/g under the conditions of 10% (v/v) CO_2 in CH_4 at 70°C, with a maximum separation coefficient of 3.9198. Moreover, cyclic CO_2 adsorption–desorption tests demonstrated the excellent regenerability and stability of Na-MCM-41(0.55), which exhibited a decrease in adsorption capacity of only 5.76% over 10 cycles.

Keywords: Na-MCM-41; Solid amine sorbent; CO_2 selective adsorption; Regeneration

_____

INTRODUCTION

The atmospheric "greenhouse effect" and global warming are the biggest environmental problems that we are facing in the 21st century. The large amount of CO_2 produced by our energy systems and discharged directly into the atmosphere is the main cause of these phenomena. Additionally, because the greenhouse effect of CH_4 is about 21 times higher than that of CO_2, CH_4 emissions are another important contributor to the greenhouse effect [1]. Therefore, from the point of view of both environmental protection and energy conservation, it is necessary to recycle and utilize CH_4 and CO_2 emissions worldwide. In recent years, China's economy has rapidly developed and the demand for natural gas has also shown rapid growth. To meet the growing demand for natural gas, it is necessary to tap the potential of existing wells to increase production and concurrently exploit more new gas fields. However, using these strategies, the quality of the obtained natural gas is becoming gradually more complex [2]. A CO_2 volume fraction of no more than 3% in natural gas is required to meet quality standard GB17820-199 [3]. Consequently, the development of methods to remove CO_2 and organic sulfur effectively while minimizing the loss of hydrocarbons is currently of great interest [4]. At present, the development of CO_2-selective adsorbents with strong adsorption capacity and stable cyclic regeneration performance is essential for handling the large volume of CO_2 from natural gas extraction. Selective CO_2 adsorption can be targeted and stabilized by utilizing functional groups, mainly amine groups, with high affinities for CO_2 on the surface of the adsorbent materials [5]. Moreover, the adsorbent material should have a large specific surface area and pore structure [6]. It has been reported that many mesoporous materials obtained through synthesis and modification of silica materials are efficient for CO_2 capture. Cavenati et al. [7]. Studied zeolite 13X as a solid adsorbent for CO_2 capture, revealing a CO_2 adsorption capacity of 28.7 wt.% and a CO_2/N_2 separation coefficient of 3.65 at 298 K and 10 bar. Jadhav et al. [8] used monoethanolamine (MEA) to

_____

modify zeolite 13X (MEA-13X) using a physical impregnation method, achieving an approximately 1.6-fold improvement in the CO_2 adsorption capacity relative to that of the unmodified material at 303 K. The improved capacity of MEA-13X indicated that chemical interactions between CO_2 and amine groups might play a key role in the adsorption process. Elkhalifah et al. [9] modified bentonite with monoethanolammonium cations to obtain a MEA^+-Mg-bentonite composite that adsorbs CO_2 reversibly and selectively over other light gases. Moreover, at a pressure of 1 bar, an equilibrium selectivity of 4.85 was observed for CO_2 over CH_4 on MEA^+-Mg-bentonite at 50°C. In this work, siliceous Na-MCM-41 was chosen as the substrate. In spite of the high present cost that is not available to large-scale synthesis, Na-MCM-41 has great potential owing to its high surface area and regular framework structure. In addition, the synthesis process for Na-MCM-41 is extremely ripe and easy to grasp. Subsequently, the Na-MCM-41 surface was functionalized with tetraethylenepentamine (TEPA) using a physical impregnation method to achieve different amine loadings. This work aimed to evaluate the effect of amine loading on CO_2 adsorption and CO_2/CH_4 separation performance, and to examine regulation of the separation performance using temperature and pressure.

EXPERIMENTAL SECTION

Chemicals
Methanol (99.5%), tetraethyl orthosilicate (TEOS) (98%) and tetraethylene pentamine (TEPA)(98%) were purchased from Sinopharm Chemical Reagent. Cetyltrimethyl Ammonium Bromide (CTAB)(98%) was supplied from Aladdin Industrial Inc. Sodium hydroxide(NaOH) was provided by Jiangsu Tong Sheng Chemicals. Distilled water was self-made in laboratory which used in all experiments.

Synthesis of Ordered Mesoporous Silicas Na-MCM-41
Ordered mesoporous silica Na-MCM-41 was prepared using a literature method with minor modifications [10]. In a typical synthesis, 2.67 g of NaOH was dissolved in 400 mL of distilled water at 40°C, and then 8.1 g of CTAB was added to the solution. When CTAB was completely dissolved, 49.97 mL of TEOS was adding drop-by-drop into this solution, which was subsequently stirred magnetically for 24 h under seal condition. The mixture was then transferred into a Teflon-lined autoclave and heated at 120°C for 48 h. afterwards; the solid product was recovered by filtration and dried at 80°C in an air blast dryer overnight. Subsequently, the product was calcined at 550°C for 6 h in air at a heating rate of 1°C/min to remove the CTAB template. This sample was denoted as Na-MCM-41

Preparation of Na-MCM-41-based Solid Amine Sorbents
Na-MCM-41-based solid amine sorbents were prepared by wet impregnation, which has been reported elsewhere [11]. In a typical preparation, a certain volume of TEPA was added to 60 mL of methanol under magnetic stirring until completely dissolved. Then, 10 g of Na-MCM-41 was added slowly to the TEPA solution under vigorously stirring for 24 h to promote the interaction between TEPA and the support. The solvent was then removed by rotary evaporation at 100°C, and the recovered solid was dried at 80°C in an air blast dryer overnight. The sample was denoted as Na-MCM-41(x), where x is the mass ratio of TEPA and the support.

Characterization of Na-MCM-41-based Solid Amine Sorbents
Na-MCM-41 and the TEPA-modified sorbents were characterized by Fourier transform infrared (FT-IR) spectroscopy using the KBr powder technique and a diffuse reflectance sampling accessory at a resolution of 4 cm^{-1} at room temperature on a Nicolet 460 spectrometer. The IR spectrum of liquid TEPA was also collected. X-ray diffraction (XRD) was used to provide further evidence for successful loading of TEPA on Na-MCM-41. The powder XRD patterns were collected using a Rigaku D/MAX-2500PC diffractometer operated at 40 kV and 40 mA with nickel-filtered Cu Kα radiation (λ = 1.5406 Å). The diffraction data were recorded in the 2θ range of 2–10° with a step size of 0.02° and a scan rate of 4°/min.

Adsorption and Recycle Measurements
The performance of the Na-MCM-41(x) sorbents for selective CO_2 capture was evaluated using a home-built fixed-bed reactor (Figure 1) that was constructed in accordance with systems reported in the literature [12]. The CO_2 concentration at the outlet was analyzed using an online multicomponent gas analyzer (DF-OMT). A simulated gas mixture of 10% CO_2 and 90% CH_4 was used as a model natural gas. In each run, about 0.25 g of dried sorbent was packed into the middle of the stainless steel tube reactor (8 mm inner diameter), and then pretreated by vacuuming to -0.10 MPa at room temperature for 10 min to remove adsorbed moisture. The sorbents were heated to the required adsorption temperature under normal pressure and the model natural gas mixture was flowed into the reactor at a flow rate of 100 mL/min. The adsorption tests were stopped when the CO_2 signal was maximized and showed no further changes. All CO_2 breakthrough curves were corrected by subtracting the mean residence time, which was determined by flowing model gas mixture through the empty

_____

reactor.

The integral equation of the breakthrough curve is displayed in Equation 1: [13]

$$Q_s = \frac{\int_o^t (u_o y_o - u_e y_e) ACdt - \frac{\varepsilon ALy_o P}{RT}}{m} \qquad (1)$$

where m is the weight of the sorbent, g; u_o and u_e are the line speeds of the inlet and outlet gases, respectively, cm/s; y_o and y_e are the percentage contents of the influent and effluent gases, respectively; A is the cross-sectional area of the fixed bed, cm^2; C is the total concentration of the gas phase, mol/L; ε is the voidage of the fixed bed; L is the length of the fixed bed, cm; P is the adsorption pressure, kPa; T is the adsorption temperature, K; R is the gas constant; and t is the adsorption time, s. Q_s is defined as the saturated adsorption capacity when y_e/y_o is equal to 0.95, while Q_b is defined as the breakthrough adsorption capacity when y_e/y_o is equal to 0.05.

The separation factor of a mixed gas adsorption system can be calculated using Equation 2: [13]

$$\partial_{ij} = \frac{\left(\frac{x}{y}\right)_i}{\left(\frac{x}{y}\right)_j} \qquad (2)$$

where x and y refer to the mole fractions of the adsorption phase and the gas phase, respectively; and i and j represent components i and j, respectively.

The regeneration performance of the Na-MCM-41(x) sorbents were investigated by releasing pre-adsorbed CO_2 by introducing inert N_2 (200 mL/min) for 10 min at 120°C. Then, the sorbents were cooled to 70°C for the second adsorption process, and the adsorption–desorption procedure was repeated ten times.
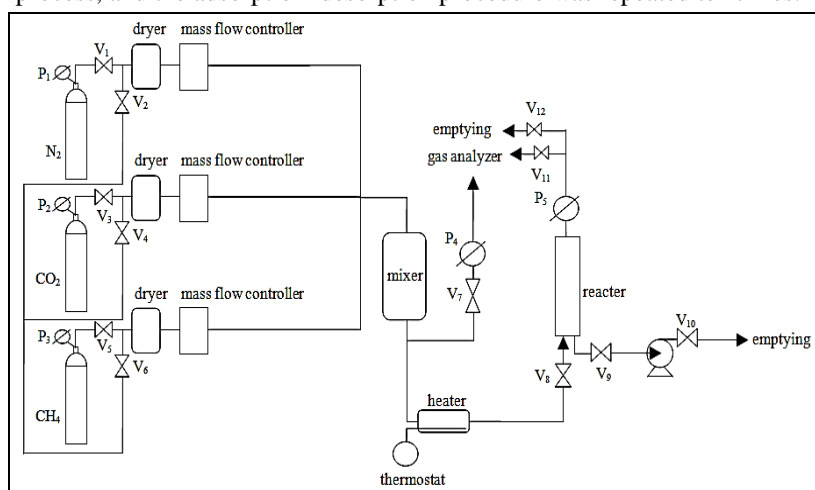
Figure 1: Schematic diagram of the home-built fixed-bed reactor

RESULTS AND DISCUSSION

Characterizations of Sorbents

The XRD patterns of the Na-MCM-41-based sorbents are shown in Figure 2. For unmodified Na-MCM-41, an obvious sharp peak was observed at $2\theta = 2.3°$, which is consistent with the (100) face of the structure of Na-MCM-41 [14]. The two weak peaks at $2\theta = 4.06°$ and $4.56°$ correspond to the (110) and (200) places of Na-MCM-41, respectively. After modification with TEPA, the two weak peaks disappeared. In contrast, the diffraction intensity of the sharp peak decreased as the TEPA loading increased, nearly disappearing at 65% loading, which might be caused by the pore-filling effect [15]. The characteristic peak of Na-MCM-41 at $2\theta = 2.4°$ shifted slightly toward larger angles after modification with TEPA, indicating successful TEPA loading, as interactions between the active component and the support result in a shift of the peak position. FT-IR spectra were obtained to further characterize Na-MCM-41 before and after TEPA loading (Figure 3). Figure 3 also shows the FT-IR spectrum of TEPA, with characteristic peaks at 3281.89 and 1591.34 cm^{-1} corresponding to N–H stretching and N–H bending vibrations, respectively [16]. The spectrum of Na-MCM-41(0.55) exhibits some of the characteristic N–H peaks of TEPA, indicating that TEPA was successfully impregnated into the support. However, the N–H stretching peak is difficult to observe in Na-MCM-41(0.55), probably because this peak is overlaid with the wide peak of surface O–H groups or adsorbed water (3000–3600 cm^{-1}) [17]. Moreover, the N–H bending vibration peak in Na-MCM-41(0.55) shifts to 1631.67 cm^{-1}, indicating an interaction between Na-MCM-41 and TEPA. Further sharp peaks in the FT-IR spectrum of TEPA at 2932, 2817, and 1452 cm^{-1}

_____

were attributed to the stretching and bending vibrations of C–H groups [18]. The observation of similar peaks in the FT-IR spectrum of Na-MCM-41(0.55) but not in that of Na-MCM-41 further supports successfully impregnation of TEPA in the support.
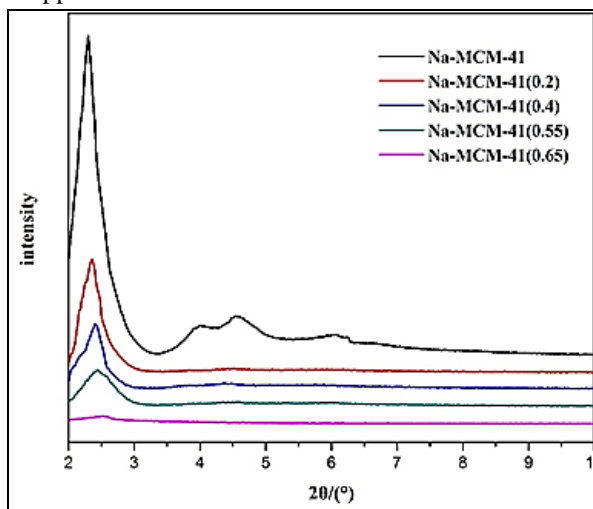
Figure 2: The XRD patterns of Na-MCM-41 and Na-MCM-41-based sorbents
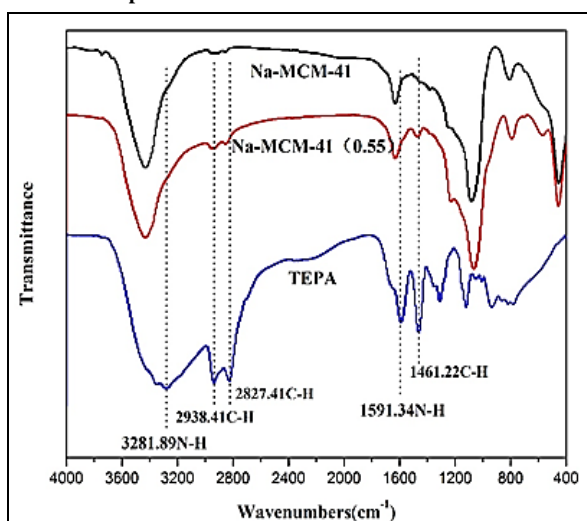
Figure 3: The FT-IR spectra of Na-MCM-41 and Na-MCM-41(0.55) and raw TEPA

N_2 adsorption–desorption isotherms of calcined Na-MCM-41 and TEPA-loaded Na-MCM-41 samples all exhibited typical type-IV behavior with a sharp inflection points at $p/p_0 > 0.3$ (Figure 4). This observation indicates the presence of mesopores in these materials and is characteristic of capillary condensation, which indicates uniformity of the mesopore size distribution. Table 1 lists the textural properties of these samples. For the TEPA-functionalized Na-MCM-41-based sorbents, the S_{BET} values and pore sizes both decrease in the order: Na-MCM-41(0.2) > Na-MCM-41(0.4) > Na-MCM-41(0.5) > Na-MCM-41(0.65), which can be attributed to the increased loading of TEPA. It is worth noting that S_{BET} of NA-MCM-41(0.65) is significantly smaller than those of the other Na-MCM-41-based sorbents, which likely contributes to the much lower separation coefficients observed at higher amine loadings (vide infra). Transmission electron microscopy (TEM)-energy-dispersive X-ray (EDX) spectroscopy analysis revealed C atoms in the TEPA-modified Na-MCM-41 adsorbents, which further indicated that TEPA has been impregnated into the support successfully. Further, the EDX results provide insight into the relationship between TEPA concentration and load capacity. An examination of four TEPA-modified Na-MCM-41 prepared with different concentrations of TEPA solution revealed that the C/Si molar ratio increased as the concentration of the TEPA solution increased. However, the C/Si ratio of Na-MCM-41(0.6) was only negligibly higher than that of Na-MCM-41(0.55), which indicated that the maximum load was basically achieved for Na-MCM-41(0.55). The EDX results also showed that there was no linear relationship between the concentration of the TEPA solution and the load capacity. Interestingly, the separation coefficient did not increase with the increasing load capacity of TEPA (vide infra).The TEM images in Figure 5a show that most TEPA loaded in Na-MCM-41(0.55) was well distributed inside the pores of Na-MCM-41. Furthermore, the ordered pore channels of the adsorbent support were evenly distributed, and consisted mainly of small micropores and mesopores (Figure 5b). The marginal area of the adsorbent could not

_____

be loaded with organic amines, as an even distribution of the pore structure of the adsorbent could be observed (Figures 5c and 5d).
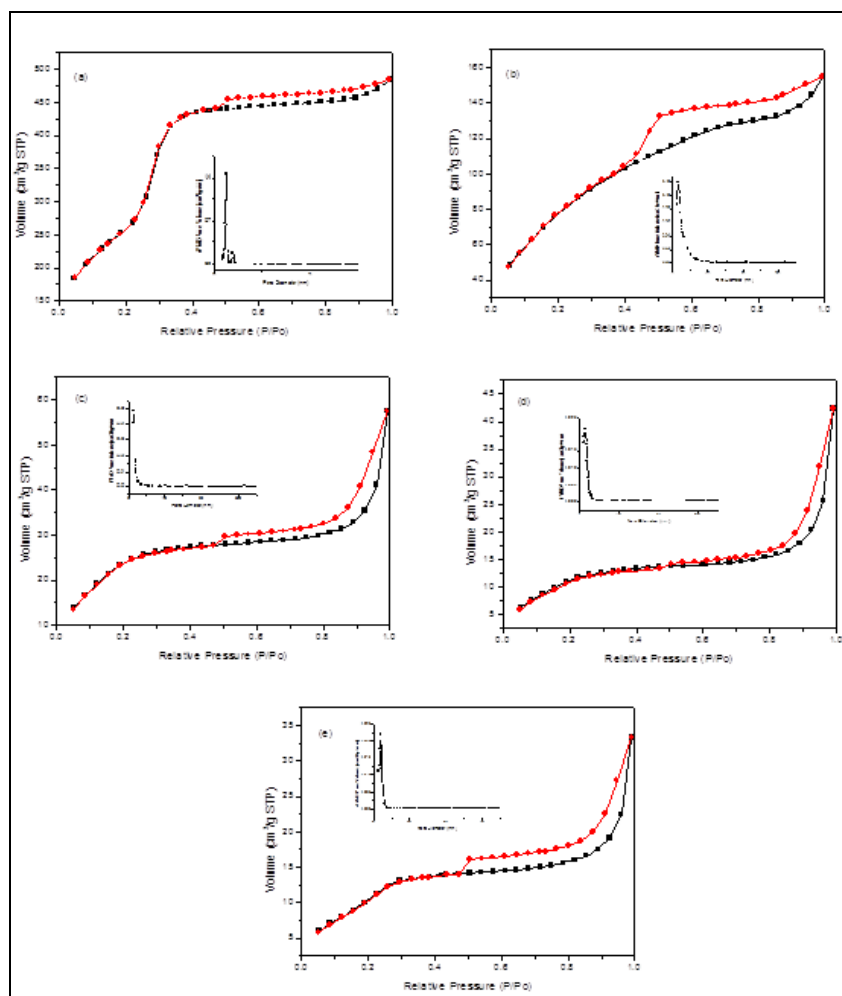
Figure 4: Nitrogen adsorption - desorption isotherms and BJH pore size distribution curves of (a) Na-MCM-41, (b) Na-MCM-41(0.2), (c) Na-MCM-41(0.4), (d) Na-MCM-41(0.55) and (e)Na-MCM-41(0.65)

Table 1: The pore structure properties of TEPA/Na-MCM-41 adsorbents

Sample	Specific surface area(m^2/g) [a]	Total pore volume (cm^3/g) [a]	Average pore Diameter (nm)[a]	C/Si (At%)[b]
Na-MCM-41	927.78	0.7	2.53	-
Na-MCM-41(0.2)	697.14	0.56	2.44	0.663
Na-MCM-41(0.4)	403.28	0.35	2.31	0.9333
Na-MCM-41(0.55)	251.44	0.16	2.26	3.1867
Na-MCM-41(0.6)	24.02	0.07	1.7	3.4264

a: Specific surface area, total pore volume and average pore diameter derived from N_2 adsorption isotherms at 77 K; b: Molar ratios measured by EDX.

CO$_2$ Selective Capture Capacities of Sorbents
Effect of the amine loading:
The CO_2 breakthrough curves of Na-MCM-41 and TEPA-modified Na-MCM-41 at 25°C are shown in Figure 6. A temperature of 25°C was chosen in accordance with previous reports [19] that indicate this is the basic temperature of adsorption tests. The inaccuracy of the mass flow controllers is ±0.35% and the measurement uncertainty is considered to be ±0.3%, resulting in a total error of 0.7% in the CO_2 adsorption capacity. For unmodified Na-MCM-41, the CO_2 breakthrough point is at approximately 70 s. After TEPA modification, the CO_2 breakthrough point increases greatly to approximately 125 s for Na-MCM-41(0.2), 150 s for Na-MCM-41(0.4), 180 s for Na-MCM-41(0.5), and 200 s for Na-MCM-41(0.55), indicating an increase in the amount of CO_2 adsorbed with increased amine loading of these composite sorbents. These results are consistent

_____

with previous reports [20]. The CO_2 saturated adsorption capacities of Na-MCM-41, Na-MCM-41(0.2), Na-MCM-41(0.4), Na-MCM-41(0.5), and Na-MCM-41(0.55) were calculated as 0.209, 0.707, 1.289, 1.774, and 2.12 mmol/g, respectively. However, at higher amine loadings, the CO_2 breakthrough point begins to decline, decreasing to approximately 120 s for Na-MCM-41(0.7) with a CO_2 saturated adsorption capacity of 1.281 mmol/g. At amine loadings of less than 55%, the mass transfer zone of the solid amine adsorbent is shorter, which means that the mass transfer resistance of the adsorbent is lower. However, at higher TEPA loadings, the pores of Na-MCM-41 are filled and the diffusion distance of CO_2 from the surface to the active site inside the pore is longer [21]. These phenomena lower the binding efficiency of the amines for CO_2, which decreases the CO_2 capture capacity.
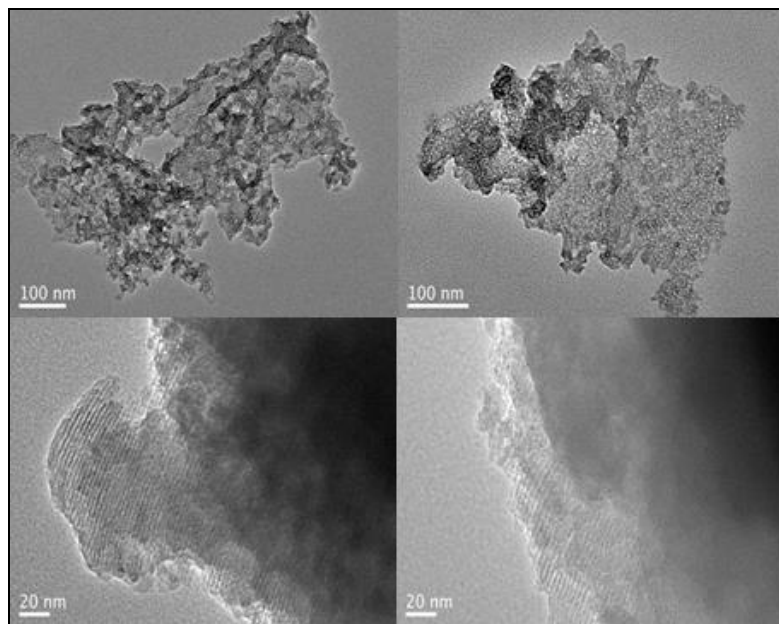
Figure 5: TEM images of Na-MCM-41(0.55)
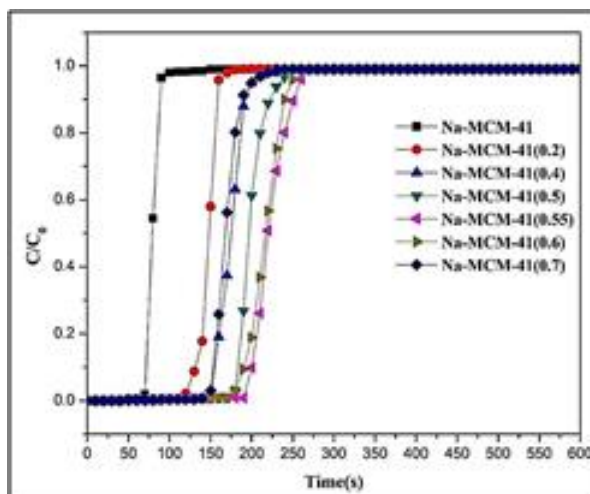
Figure 6: CO_2 breakthrough curves of Na-MCM-41 and amine modified Na-MCM-41

The CO_2/CH_4 breakthrough curves of Na-MCM-41 and Na-MCM-41(0.55) at 25°C are shown in Figures 7 and 8, respectively. The selective adsorption of CO_2 from a CO_2/CH_4 gas mixture is obviously improved on Na-MCM-41(0.55). The breakthrough times of CO_2 and CH_4 are about 21 and 80 s on Na-MCM-41, respectively, and increase to 30 and 195 s, respectively, after loading with 55% TEPA. The separation coefficients on Na-MCM-41 and Na-MCM-41(0.55) were calculated as 0.2718 and 1.334, respectively. The effects of TEPA loading on the adsorption properties of Na-MCM-41 are summarized in Table 2.

_____
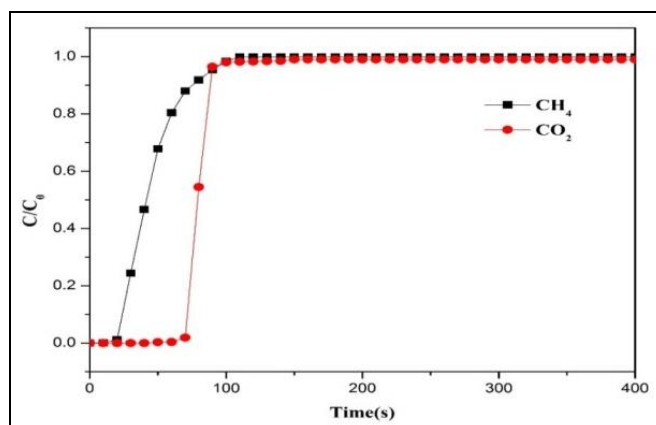
Figure 7: CO₂/CH₄ breakthrough curves of Na-MCM-41
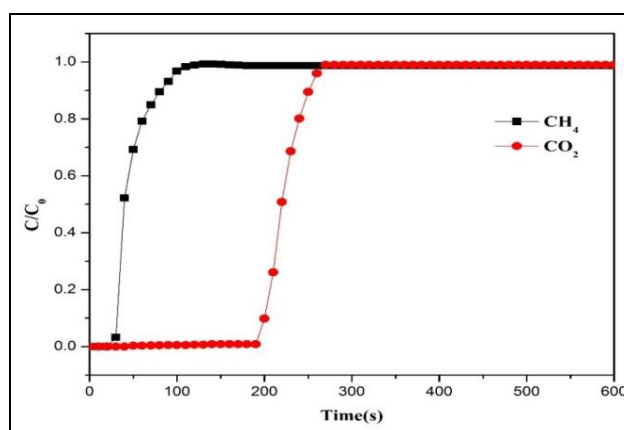
Figure 8: CO₂/CH₄ breakthrough curves of Na-MCM-41(0.55)

Table 2: Effect of Na-MCM-41(0.55) on the adsorption capacity properties

Sample	t_b of CH_4	t_b of CO_2	Q_s of CH_4	Q_s of CO_2	α
Na-MCM-41	21s	80s	0.085311	0.208699	0.2718
Na-MCM-41(0.55)	30s	195s	0.176603	2.12035	1.334

Effect of the adsorption temperature:

The adsorption temperature has an important influence on the CO_2 adsorption process. In this study, the effect of temperature (25, 40, 55, 70, 85, and 100°C) on the selective adsorption performance of Na-MCM-41(0.55) was investigated at a feed flow rate of 100 mL/min and atmospheric pressure. Figure 9 shows the effect of temperature on the adsorption capacities of CO_2 and CH_4. The CO_2 adsorption capacity increased as the temperature increased, reaching a maximum at 70°C. With further increases in temperature from 70 to 100°C, the CO_2 adsorption performance obviously decreased. This tendency agrees well with previous reports [22]. The CO_2 adsorption process is affected by both dynamics and thermodynamics [23]. As the adsorption of CO_2 on Na-MCM-41(0.55) is an exothermic reaction, a low temperature is beneficial for this process. However, the active component, TEPA, is a highly viscous organic amine. When the temperature is increased to 70°C, TEPA becomes more flexible and can disperse more uniformly on the support, facilitating the reaction between CO_2 and the binding sites in Na-MCM-41(0.55). Accordingly, the adsorptive reaction was primarily determined by dynamics below 70°C, but thermodynamics dominated the reaction when the temperature was further increased to 100°C, resulting in the decreased adsorption capacity. Furthermore, the CH_4 adsorption capacity showed a gradual decrease as the temperature increased, probably because the adsorption of CH_4 on Na-MCM-41(0.55) was extremely weak, and the temperature increase would accelerate the diffusion rate of CH_4. The effect of the adsorption temperature on the separation coefficient is summarized in Table 3.

Table 3: Effect of adsorption temperature on the separation coefficient

T	25°C	40°C	55°C	70°C	85°C	100°C
α	1.334	1.7748	2.9022	3.9198	3.6302	3.2337

_____
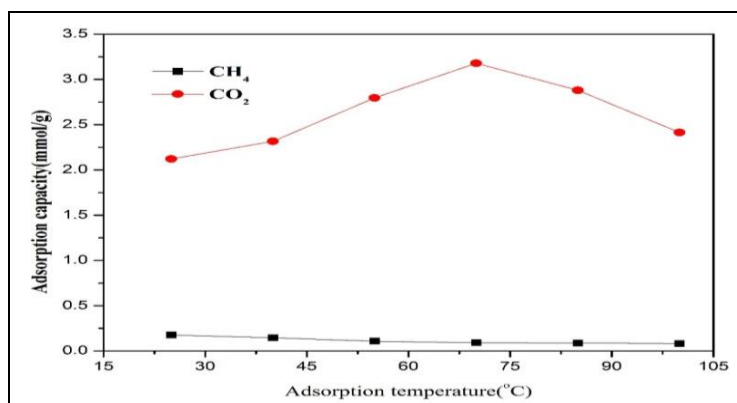
Figure 9: The adsorption capacity of Na-MCM-41(0.55) at different adsorption temperatures

Cyclic adsorption-desorption study of Na-MCM-41(0.55):

In real industrial applications, a high adsorption capacity along with good regenerability of the sorbent during cyclic adsorption–desorption process are important. Therefore, to evaluate the stability and regenerability of Na-MCM-41(0.55), cyclic CO_2 adsorption-desorption processes were carried out for 10 consecutive runs. The saturated adsorption capacity after each cycle is shown in Figure 10. After 10 cycles, the adsorption capacity decreased from 3.178 to 2.995 mmol/g, which is a decrease of only 5.76%. This loss in CO_2 capacity during the cyclic tests could be caused by continuous volatilization of doped TEPA [24] or the generation of urea groups, which are inactive for CO_2 adsorption, during the CO_2 desorption process [25]. Overall, Na-MCM-41(0.55) has quite stable CO_2 uptake, demonstrating its excellent regenerability and stability during multiple cyclic operations.
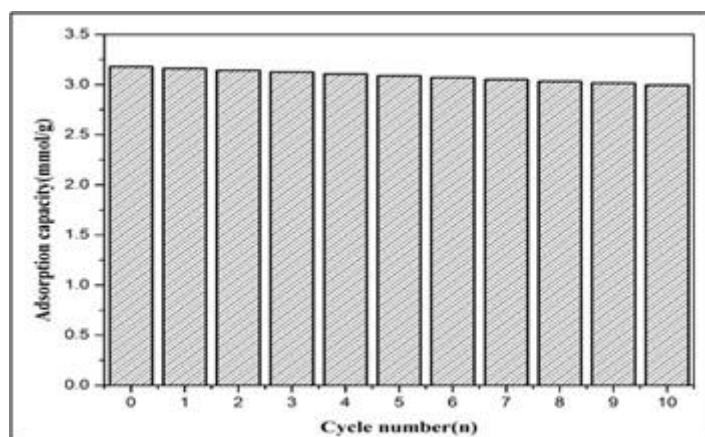
Figure 10: The cyclic adsorption-desorption of Na-MCM-41(0.55) under 10%CO_2/CH_4 at 70℃

CONCLUSION

Ordered mesoporous Na-MCM-41 was shown to be a good support for high TEPA loading levels to fabricate solid amine-supported composite adsorbents with high CO_2 uptakes. TEPA is a liquid with a high amine density, but its dispersion on the support is limited owing to its high viscosity. However, under optimized operating conditions at 70°C, Na-MCM-41(0.55) exhibited a maximum CO_2 adsorption capacity and separation coefficient of 3.178 mmol/g and 3.9198, respectively, which are significantly higher than the corresponding values for the unmodified support. Moreover, Na-MCM-41(0.55) demonstrated good regenerability over 10 adsorption–desorption cycles in the temperature range of 70°C (adsorption) to 120°C (desorption), with a decrease in adsorption capacity of only 5.76%.

ACKNOWLEDGEMENT

_____

REFERENCES

[1]   M Masoud; G Fatemeh. *Micropor Mesopor Mat*. **2014**, 200, 1-10.

[2]   M Patricia. *Master in Chemical Engineering thesis*.University of Porto, **2011**.

[3]   Y Zhu; L Guo. *J Modern Chem Ind*. **2015**, 35(2), 125-128.

[4]   X Sun; M Zhang. *J Nat Gas Chem Ind*. **2013**, 38(5), 91-94.

[5]   T Prenzel; M Wilhelm; K Rezwan. *Chem Eng J*. **2014**, 235, 198.

[6]   L Wang; M Yao; X Hu; G Hu; J Lu; M Luo; M Fan. *Applied Surface Sci*. **2015**, 324, 286-292.

[7]   S Cavenati; CA Grande; AE Rodrigues. *J Chem Eng Data*. **2004**, 49, 1095.

[8]   PD Jadhav; RV Chatti; RB Biniwale; NK Labhsetwar; S Devotta; SS Rayalu. *Energ Fuels*. **2007**, 21, 3555.

[9]   EI Ali; M Elkhalifah; AM Azmi Bustam; T Shariff; T Murugesan. *Applied Clay Sci*. **2015**, 107, 213-219.

[10]   F Xin; D Wang. *New Chem Mat*. **2015**, 43(8), 163-165.

[11]   M Yao; Y Dong; X Hu; X Feng; A Jia; G Xie; GS Hu; J Lu; M Luo; M Fan. *Energy Fuels*. **2013**, 27, 7673-7680.

[12]   M Yao; Y Dong; J Xie; A Jia; G Xie; GS Hu; M Luo. *Acta Physico-Chimica Sinica*. **2014**, 30, 789-796.

[13]   R Hongzheng; Z Yaping. Studies on adsorption separation of CO_2/N_2 mixed gases. Tianjin University, **2010**, 6.

[14]   M Sarmah; BP Baruah; P Khare. *Fuel Process Technol*. **2013**,106, 490-497.

[15]   X Xu; C Song; JM Andresen; BG Miller; AW Scaroni. *Energy Fuels*. **2002**, 16, 1463-1469.

[16]   L Guo; X Hu; G Hu; J Chen; Z Li; W Dai; M Fan. *Fuel Processing Technol*. **2015**.

[17]   X Zhao; X Hu; G Hu; R Bai; W Dai; M Fan; M Luo. *J Mater Chem*. **2013**, 1, 6208-6215.

[18]   XX Feng; GS Hu; X Hu; GQ Xie; YL Xie; JQ Lu; MF Luo. *Ind Eng Chem Res*. **2013**, 52, 4221-4228.

[19]   G Qi; Y Wang; L Estevez; X Duan; N Anako; AHA Park; W Li; CW Jones; EP Giannelis. *Energy Environ Sci*. **2011**, 4, 444-452.

[20]   X Ma; X Wang; C Song. *J Am Chem Soc*. **2009**, 131, 5777-5783.

[21]   J Wang; L Lin. East China University of Science and Technology. **2013.**

[22]   X Wang; L Chen; Q Guo. *Chem Eng J*. **2015**, 260, 573-581.

[23]   W Xia; G Qingjie; Z Jun; C Linlin. *Int J Greenhouse Gas Control*. **2015**, 37, 90-98.

[24]   G Qi; L Fu; BH Choi; EP Giannelis. *Energy Environ Sci*. **2012**, 5, 7368-7375.

[25]   A Sayari; Y Belmabkhout. *J Am Chem Soc*. **2010**,132, 6312-6314.